CONDENSED MATTER PHYSICS

Light-induced magnetization from magnonic rectification

Tom Kahana[1]†, Daniel A. Bustamante Lopez[2]†, Dominik M. Juraschek[1]*

Rectification describes the conversion of an oscillating field or current into a quasi-static one and the most basic example of a rectifier is an AC/DC converter in electronics. This principle can be translated to nonlinear light-matter interactions, where optical rectification converts the oscillating electric field component of light into a quasi-static polarization and phononic rectification converts a lattice vibration into a quasi-static structural distortion. Here, we present a rectification mechanism for magnetism that we call magnonic rectification, where a spin precession is converted into a quasi-static magnetization through the force exerted by a coupled chiral phonon mode. The transiently induced magnetic state resembles that of a canted antiferromagnet, opening an avenue toward creating dynamical spin configurations that are not accessible in equilibrium.

INTRODUCTION

Rectification conventionally describes the process of converting a time-dependent, alternating current (AC) into a quasi-static, direct current (DC). While rectifiers are ubiquitous in modern electronic devices, the concept of AC/DC conversion can be extended to collective excitations induced by light in a nonlinear medium. In nonlinear optics, optical rectification describes the conversion of the oscillating electric field component of light into a quasi-static polarization in the material, which has become one of the most important mechanisms for the generation of terahertz radiation today (*1*). In nonlinear phononics, phononic rectification describes the conversion of a coherent lattice vibration into a quasi-static structural distortion (*2*, *3*). The latter has led to astonishing discoveries in recent years, including light-induced and enhanced superconductivity (*4*–*7*), ferroelectricity (*8*–*14*), and magnetism (*15*–*23*). With these developments as a background, our present study asks the question: Does an analog mechanism also exist for magnons, which are collective spin precessions in magnetic materials? Here, we theoretically demonstrate magnonic rectification in an antiferromagnetic material, in which a spin precession is converted into a transient spin canting, generating a quasi-static magnetization in the process (see Fig. 1). The rectification is achieved through the effective magnetic field produced by a laser-excited chiral phonon mode, which has recently been predicted and measured in various materials (*24*–*35*). The resulting nonequilibrium magnetic state resembles a canted antiferromagnet or weak ferromagnet (*36*), whose direction of magnetization can be reversed by changing the helicity of the laser pulse.

RESULTS

We begin by introducing the physical basis of magnonic rectification by chiral phonons. The microscopic interaction underlying the rectification process is given by angular momentum coupling between a chiral phonon mode and the spins of the magnetic material, $\mathbf{L}_{\mathrm{ph}} \cdot \mathbf{S}$. The interaction can be written in terms of an effective magnetic field produced by the chiral phonon mode that couples to the magnetic moment of a magnon mode, $\mathbf{L}_{\mathrm{ph}} \cdot \mathbf{S} \sim \mathbf{B}_{\mathrm{ph}} \cdot \mathbf{m}$. When the chiral phonon mode is excited coherently by an ultrashort laser pulse, it exerts a force on the spins, canting them and tilting the axis of spin precession along the eigenvectors of the magnon mode. This induces a magnetization proportional to the angular momentum of the chiral phonon mode, $\langle M \rangle \propto L_{\mathrm{ph}}$ in a fundamentally nonequilibrium and nonthermal process.

Model for chiral phonon-spin dynamics

We next derive a model for the coupled phonon-magnon dynamics. We investigate the general example of an antiferromagnetic Heisenberg model with easy-plane anisotropy, which provides a common representation of many antiferromagnetic materials, such as nickel oxide or manganese oxide (*37*). For two sublattice spins aligned along the z direction, $\mathbf{S}_s$ with $s \in \{1,2\}$, the Hamiltonian reads

$$H_0 = J\mathbf{S}_1 \cdot \mathbf{S}_2 + \sum_{s=1,2} \left(D_x S_{s,x}^2 + D_y S_{s,y}^2 \right) \tag{1}$$

where J is the antiferromagnetic exchange interaction and D_x and D_y are the anisotropy energies. The relative orientation of the easy plane within the crystal is dependent on the material. In general, for $D_x < D_y$, these systems host low- and high-frequency magnon modes with eigenfrequencies of $\hbar\Omega_{\mathrm{l}} = 2\sqrt{(J+D_y)D_x}$ and $\hbar\Omega_{\mathrm{h}} = 2\sqrt{(J+D_x)D_y}$. The spin configuration is illustrated in Fig. 2. At the same time, the full phonon-dependent potential energy is given by

$$V_{\mathrm{ph}} = V_0 + V_{\mathrm{s-ph}} + V_{\mathrm{l-m}} \tag{2}$$

The first term, $V_0 = \Omega_0^2 \left(Q_y^2 + Q_z^2 \right)/2$, is the potential energy of a doubly degenerate phonon mode in the yz plane, where Ω_0 is the eigenfrequency and Q_y and Q_z are the phonon amplitudes of the two orthogonal components. A circular superposition of these components results in a chiral phonon mode, as shown in Fig. 2. These degenerate chiral phonon modes live near the center of the Brillouin zone, where they can be excited with light. Nondegenerate chiral phonon modes, such as in hexagonal two-dimensional materials or chiral crystals (*38*–*41*), are not considered here.

The second term, $V_{\mathrm{s-ph}} = -\mathbf{B}_{\mathrm{ph}} \cdot \mathbf{m}$, describes the interaction of the effective phono-magnetic field, $\mathbf{B}_{\mathrm{ph}}$, with the magnetic moment of the magnon mode, $\mathbf{m}$. $\mathbf{B}_{\mathrm{ph}} = \mu_0 \gamma_{\mathrm{ph}} \mathbf{L}_{\mathrm{ph}} / V_{\mathrm{c}}$, where γ_{ph} is the gyromagnetic

[1]School of Physics and Astronomy, Tel Aviv University, Tel Aviv 6997801, Israel. [2]Department of Physics, Boston University, Boston, MA 02215, USA.
*Corresponding author. Email: djuraschek@tauex.tau.ac.il
†These authors contributed equally to this work.

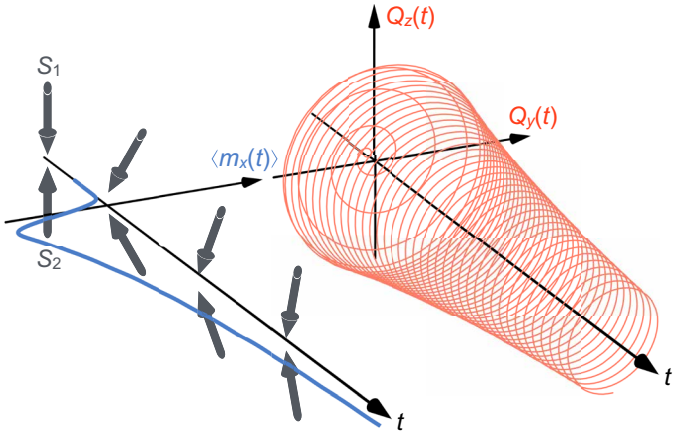

Fig. 1. Magnonic rectification by chiral phonons. Dynamical responses of the two orthogonal components of a laser-excited chiral phonon mode, $Q_y(t)$ and $Q_z(t)$, and the average magnetization component of a magnon mode coupled to it, $\langle m_x(t)\rangle$. The axis of spin precession is transiently tilted, leading to a light-induced canted antiferromagnetic state, producing a quasi-static magnetization in the system.

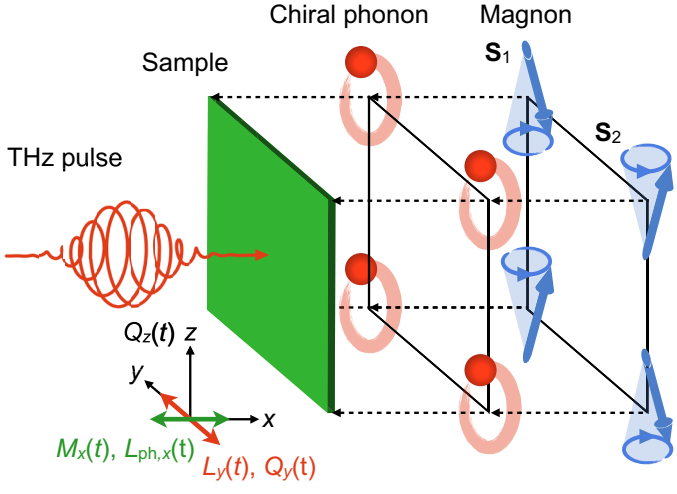

Fig. 2. Schematic of an antiferromagnetic system hosting a chiral phonon mode. We show the circular motions of the magnetic ions along the eigenvectors of the two components of the chiral phonon mode, Q_y and Q_z, in the yz plane. The phonon angular momentum, $L_{ph,x}$, accordingly points along the x axis. We further show the spin precession along the eigenvectors of the high-frequency magnon mode, with the magnetization, M_x, pointing in the x direction and the Neél vector, L_y, pointing in the y direction.

ratio of the chiral phonon, μ_0 is the vacuum permeability, and V_c is the unit-cell volume. $\mathbf{L}_{ph} = \mathbf{Q} \times \dot{\mathbf{Q}}$ is the phonon angular momentum, where $\mathbf{Q} = (0, Q_y, Q_z)$. The magnetic moment of the magnon mode is given by $\mathbf{m} = \gamma_{el}\hbar(\mathbf{S}_1 + \mathbf{S}_2)$, where γ_{el} is the gyromagnetic ratio of the electron. Using these relations, the potential can equivalently be written as an angular momentum coupling, $V_{s-ph} = k\mathbf{L}_{ph} \cdot \mathbf{S}$, where $k = -\mu_0\gamma_{ph}\gamma_{el}\hbar/V_c$ is the coupling coefficient. The effective phono-magnetic field depends on the microscopic origin of γ_{ph} and, therefore, k and can generally stem from a variety of not only electron-phonon, spin-phonon, and orbit-phonon interactions (*29*, *32*, *42*–*51*) but also phonon-magnon coupling (*27*, *52*). The direct and real magnetic field induced by the chiral phonon mode due to ionic charge currents is usually negligible compared to the effective magnetic fields (*25*, *26*, *28*, *31*, *35*, *53*). Our formalism is independent of the type of interaction as long as it takes the form of the chiral phonon-magnon coupling specified by V_{s-ph}. Without loss of generality, we choose the chiral phonon mode to be circularly polarized in the yz plane ($\mathbf{L}_{ph} \parallel \hat{\mathbf{x}}$), coupling to the magnetic moment of the high-frequency magnon mode, $\mathbf{m} = (m_x,0,0)$, as illustrated in Fig. 2. To couple to the low-frequency magnon mode, the circular polarization would need to be in the xz plane ($\mathbf{L}_{ph} \parallel \hat{\mathbf{y}}$).

The third term, $V_{l-m} = -(\mathbf{p}_y + \mathbf{p}_z) \cdot \mathbf{E}(t)$, describes the light-matter interaction of the chiral phonon mode with the laser pulse and is given by electric-dipole coupling. $\mathbf{p}_n = \mathbf{Z}_n Q_n$ is the electric dipole moment of the phonon component $n \in \{y, z\}$, $\mathbf{Z}_n$ is the mode effective charge, and $\mathbf{E}(t)$ is the electric field component of the laser pulse. We use the Einstein sum convention for summing over spatial indices. $Z_{n,i}$ is nonzero if the driven phonon mode is infrared-active and the coordinate system can be chosen such that $n \equiv i$.

The coherent spin dynamics in the macrospin approximation are described by the Landau-Lifshitz-Gilbert equations (*37*, *54*)

$$\frac{d\mathbf{S}_s}{dt} = \frac{\gamma_{el}}{1+\kappa_{el}^2}\left[\mathbf{S}_s \times \mathbf{B}_s^{eff} - \frac{\kappa_{el}}{|\mathbf{S}_s|}\mathbf{S}_s \times \left(\mathbf{S}_s \times \mathbf{B}_s^{eff}\right)\right] \quad (3)$$

where κ_{el} is the Gilbert damping (*55*, *56*) and the spin vectors are normalized, $|\mathbf{S}_s| = 1$. $\mathbf{B}_s^{eff} = -\left(\gamma_{el}\hbar\right)^{-1}\partial_{\mathbf{S}_s} H$ is the effective magnetic field acting on the spins of sublattice s, with the full spin-dependent Hamiltonian given by $H = H_0 + V_{s-ph}$. The effective phono-magnetic field $\mathbf{B}_{ph}$ enters the Landau-Lifshitz-Gilbert equations as a part of $\mathbf{B}_s^{eff}$. Coherent phonon dynamics can be described by a phenomenological oscillator model (*3*, *6*, *15*, *57*, *58*), and we capture the coupled equations using the damped Euler-Lagrange equations

$$\frac{d}{dt}\frac{\partial \mathscr{L}}{\partial \dot{Q}} - \frac{\partial \mathscr{L}}{\partial Q} = -\frac{\partial G}{\partial \dot{Q}} \quad (4)$$

Here, $\mathscr{L} = \left(\dot{Q}_y^2 + \dot{Q}_z^2\right)/2 - V_{ph}$ is the phonon Lagrangian, and $G = \kappa_0\left(\dot{Q}_y^2 + \dot{Q}_z^2\right)/2$ is the Rayleigh dissipation function with $\kappa_y = \kappa_z \equiv \kappa_0$ as the phonon linewidth (see the Supplementary Materials for details of the equations.)

Quasi-static magnetization and nonlinear magnetoelectric susceptibility

We now derive an expression for the average magnetization of the magnon mode that obtains a nonzero value in the presence of a coherent chiral phonon, $\langle M_x\rangle \neq 0$. We minimize the full spin-dependent Hamiltonian, $H = H_0 + V_{s-ph}$, for spin canting along the magnon eigenvectors and use $\langle M_x\rangle = \langle m_x\rangle/V_c$ to obtain

$$\langle M_x\rangle = -\frac{\gamma_{el}\hbar}{V_c}\frac{k}{J + D_x}L_{ph,x} \quad (5)$$

The spins are canted by a mean tilt angle $\langle\theta\rangle \neq 0$, and the average value of the induced magnetization is proportional to the phonon angular momentum, $\langle M_x\rangle \propto L_{ph,x}$. Equation 5 is a quasi-static snapshot of the time-dependent system and valid for small-angle deviations, $\theta \ll 90°$, which holds for all physical values of $L_{ph,x}$.

We obtain the full spin-dynamical response to the coherent chiral phonon excitation by solving the Landau-Lifshitz-Gilbert equations for the high-frequency magnon mode in frequency space to linear

order in the effective phono-magnetic field (see the Supplementary Materials for details of the derivations), yielding

$$M_x(\omega) = \frac{1}{\sqrt{2\pi}} \int_{-\infty}^{\infty} \chi^{(2)}_{xjk}(\omega, \omega') E_j(\omega - \omega') E_k(\omega') d\omega \quad (6)$$

The magnetization takes the form of a second-order nonlinear magneto-optical response, where $\chi^{(2)}_{xjk}$ is the nonlinear magnetoelectric susceptibility given by

$$\chi^{(2)}_{xjk}(\omega, \omega') = C \times \frac{\epsilon_{xjk}(i\kappa_{el}\omega + 2D_y/\hbar) i\omega'}{\Delta_m(\omega)\Delta_0(\omega - \omega')\Delta_0(\omega')} \quad (7)$$

Here, $\Delta_\alpha(\omega) = \Omega_\alpha^2 - \omega^2 + i\kappa_\alpha\omega$ is the Fourier transform of the time propagator, $d^2/dt^2 + \kappa_\alpha d/dt + \Omega_\alpha^2$, and ϵ_{xjk} is the Levi-Civita tensor. The prefactor C contains the phonon and electron gyromagnetic ratios, dampings, and mode effective charges, and Δ_m contains the magnon frequency and damping. The biggest contribution comes from the resonant driving of the chiral phonon mode at $\omega' = \Omega_0$. In the purely displacive limit, the nonlinear magnetization and susceptibility in Eqs. 6 and 7, arising from magnon-chiral phonon coupling, can be written as a rectification process analogously to the formalism of the nonlinear polarization in optical rectification (*59*, *60*) and the nonlinear displacement in phononic rectification (see the Supplementary Materials)

$$M_x(0) = \chi^{(2)}_{xjk}(0; \omega_0, -\omega_0) E_j(\omega_0) E_k^*(\omega_0) \quad (8)$$

This magnetization directly corresponds to a quasi-static tilting of the spins along the eigenvectors of the magnon mode. In a similar fashion, a quasi-static displacement of atoms along the eigenvectors of a phonon mode is induced in phononic rectification (*61*, *62*). The process can therefore be considered as magnonic rectification mediated by chiral phonons.

Simulation of magnonic rectification

We now evaluate the coupled spin-lattice dynamics that follow the coherent excitation of the chiral phonon mode, described by Eqs. 3 and 4 and the setup in Fig. 2. We use common values for the parameters of the spin Hamiltonian and phonon potential (*26*, *28*, *37*, *54*) and of the phonon gyromagnetic ratio (*29*, *31*–*34*, *43*–*46*, *51*, *52*), shown in Table 1. The circularly polarized electric field component of the ultrashort laser pulse is given by $\mathbf{E}(t) = \left(E(t)\cos(\omega_0 t), E(t)\sin(\omega_0 t), 0\right)/\sqrt{2}$, with $E(t) = E_0 \exp\left\{-t^2/\left[2\left(\tau_0/\sqrt{8\ln 2}\right)^2\right]\right\}$. We use a central frequency of $\omega_0 = \Omega_0$, a peak electric field of $E_0/\sqrt{2} = 10$ MV/cm, and a full width at half maximum duration of $\tau = 250$ fs, parameters that lie well within experimentally achievable pulse intensities (*7*, *63*).

In Fig. 3, we present the results of the dynamical simulations. Figure 3A shows the time evolution of the phonon amplitudes, Q_y and Q_z, separated by a $\phi = \pi/2$ phase shift, resulting in circular polarization. These amplitudes correspond to ionic motions of a few percentage of the interatomic distance in typical transition-metal oxide compounds and lie well within the Lindemann stability limit (*57*). In Fig. 3B, we show the time evolution of the effective magnetic field generated by the chiral phonon mode, $B_{ph,x}$, which reaches a maximum amplitude of 13.5 T before decaying quadratically as a function of the phonon amplitudes and, therefore, the phonon lifetime. The direction of the magnetic field can be reversed by changing the helicity of the laser pulse and, therefore, of the chiral phonon mode. In Fig. 3C, we show the time evolution of the magnetization induced by the spin precession of the high-frequency magnon mode for left- and right-handed circular excitations. The quasi-static shift away from the equilibrium position is clearly visible, reaching a transient maximum of $\langle M_x \rangle = 0.03\ \mu_B/V_c$. This quasi-static component leads to a net magnetization in the system after time averaging, in contrast to regular coherent spin precession dynamics (*54*, *64*). The quasi-static component decays on the timescale of the effective phono-magnetic field. In Fig. 3D, we show the normalized Fourier transforms of the time traces in Fig. 3 (A to C). There is a sharp and symmetric peak at the eigenfrequency of the chiral phonon mode, which points toward the fact that the back action of the spin system in the phonon equations of motion (*4*) is negligible. The effective phono-magnetic field shows a broadened static component at zero frequency, corresponding to the unidirectional force it exerts on the spins. The Fourier transform of the magnon mode shows three contributions: first, a sharp peak at its eigenfrequency, corresponding to the oscillatory spin precession; second, a static component at zero frequency, corresponding to the rectified, quasi-static shift; and, third, a component at the double frequency of the chiral phonon mode, $2\Omega_0$, corresponding to second-harmonic generation (SHG). The latter feature is not resolved in the linear scaling of the Fourier spectrum but can be seen in Fig. 3E, where we show the absolute value of the nonlinear magnetoelectric susceptibility for resonant driving conditions of the chiral phonon mode, $|\chi^{(2)}_{xyz}(\omega, \omega' = \Omega_0)|$, on a logarithmic scale. The three features of rectification (Rect.), oscillation (Osc.), and SHG are clearly visible. In principle, resonant conditions for coherent magnon excitation are achieved when the phonon frequency is half of the magnon frequency, which moves the oscillation and SHG peaks on top of each other. Because the SHG component of the circular excitation is orders of magnitude smaller than the difference-frequency component, the overall efficiency for this process is rather low. Last, in Fig. 3F, we show the trajectories of the sublattice spin precessions, $\mathbf{S}_1$ and $\mathbf{S}_2$, for the first precession period. The spin arrows indicate the quasi-static spin canting and tilt of the axis of spin precession, amounting to an angle of $\langle\theta\rangle = 0.5°$ at its maximum, comparable to the spin canting

Table 1. Parameters used in the dynamical simulations. *e* is the elementary charge, and *u* is the atomic mass unit.

J	D_x	D_y	$\Omega_h/(2\pi)$	γ_{el}	V_c
106 meV	160 μeV	3.5 μeV	2 THz	-2.2×10^{11} (Ts)$^{-1}$	35 Å^3
κ_{el}	$\Omega_0/(2\pi)$	κ_0	$Z_{n,i}$	γ_{ph}	
2.4×10^{-4}	10 THz	0.5 THz	$1\,e/\sqrt{u}$	10^{11} (Ts)$^{-1}$	

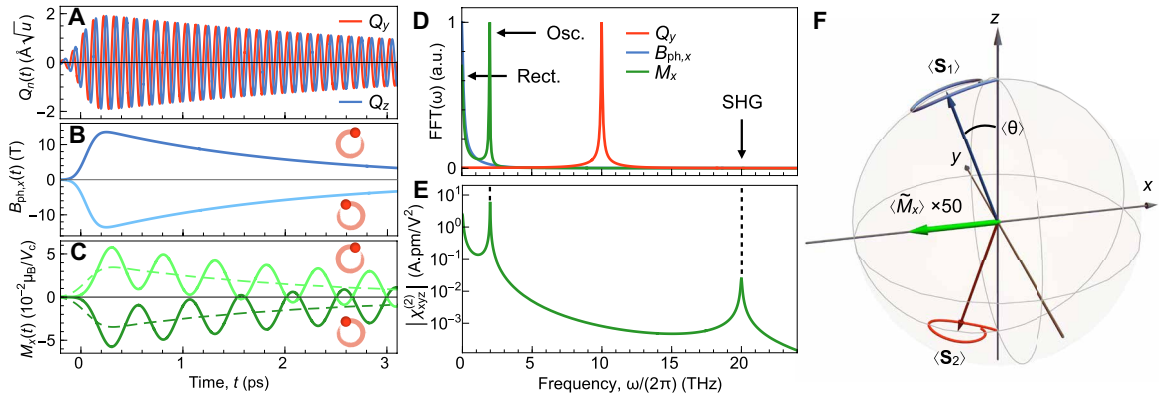

Fig. 3. Simulations of magnonic rectification. (**A**) Time-dependent phonon amplitudes of the two components of the chiral phonon mode, Q_y and Q_z, excited by a circularly polarized laser pulse at $t = 0$. (**B**) Time evolution of the effective magnetic field generated by the chiral phonon mode, $B_{ph,x}$. The direction of the phono-magnetic field depends on the helicity of the chiral phonon mode. (**C**) Time-dependent magnetization, M_x, induced by the spin precession of the high-frequency magnon mode, dependent on the helicity of the excitation. The dashed line marks the quasi-static DC component of the magnetization. (**D**) Normalized Fourier transforms of the time traces in (A) to (C). a.u., arbitrary units; FFT, fast Fourier transform. (**E**) Absolute value of the nonlinear magnetoelectric susceptibility under resonant driving conditions of the chiral phonon mode, $|\chi^{(2)}_{xyz}(\omega, \omega' = \Omega_0)|$. (**F**) Spin precession along the eigenvectors of the high-frequency magnon mode. Red and blue arrows show the transient tilting of the axis of spin precession by an angle $\langle\theta\rangle$. The trajectories on the Bloch sphere cover the first full precession period. The green arrow shows the quasi-static component of magnetization, $\langle \tilde{M}_x \rangle = \langle M_x \rangle V_c / (\gamma_{el}\hbar)$, exaggerated by a factor of 50.

commonly found in weak ferromagnets (*65*). This quasi-static canting does not appear in regular coherent magnon excitations, in which the spins precess around their respective equilibrium positions. Again, the direction of spin canting and, therefore, of the tilt angle can be reversed by changing the helicity of the chiral-phonon excitation.

DISCUSSION

We have considered the example of an antiferromagnetic Heisenberg model with easy-plane anisotropy in our study, for which nickel oxide (NiO) and manganese oxide (MnO) are promising candidates to realize magnonic rectification. NiO follows precisely the symmetry requirements of Fig. 2 and has a tiny monoclinic distortion (*64*), slightly breaking the degeneracy of the chiral phonon mode. Magnonic rectification can nevertheless be achieved as long as the dephasing time of the two components is longer than the phonon lifetime, $2\pi\left(\Omega_y - \Omega_z\right)^{-1} > \kappa^{-1}_{y/z}$, which is the case for NiO. Our results are further readily extendable and generalizable to all antiferromagnetic materials that have degenerate or nearly degenerate chiral phonon modes with the required symmetry to couple to a corresponding magnon mode. This includes compounds in the cubic, tetragonal, hexagonal, and trigonal crystal systems (degenerate), as well as orthorhombic, monoclinic, and triclinic crystal systems (nearly degenerate). A particularly interesting candidate is antiferromagnetic $CoTiO_3$, which hosts infrared-active chiral phonon modes and antiferromagnetic spins in the geometry shown in Fig. 2 and which has very recently been shown to have large phonon magnetic moments and, therefore, strong coupling to spin degrees of freedom (*51*, *66*).

As circularly polarized terahertz pulses with high electric field strengths have become feasible lately (*31*, *33*), we expect that magnonic rectification can be realized in state-of-the-art pump-probe setups. As the mechanism is based on nonlinear chiral phonon-magnon coupling, it requires exciting the chiral phonon mode with sufficiently large amplitudes, which is possible with ultrashort and highly intense laser pulses. The magnitude of the effect is ultimately limited by the damage threshold of the crystal, given by the net energy deposited by the laser pulse.

We distinguish the mechanism from other forms of spin dynamics. A direct excitation of the magnon mode through the magnetic field component of light (*54*, *67*) can be excluded because our ultrashort pulses are far off resonance from the magnon eigenfrequencies. Furthermore, the laser pulse can excite the magnon modes through the inverse Faraday or Cotton-Mouton effects (*64*, *68*), which will always occur in parallel to the proposed mechanism here, if the selection rules of the magnetic Raman tensor allow for it. In general, optomagnetic effects produce effective magnetic fields that induce low-frequency spin dynamics (*69*, *70*) and contribute to the amplitude of the spin precession but do not induce quasi-static tilting of the axis of precession. Magnetization can be transiently generated in antiferromagnets through piezomagnetically active phonon modes (*18*, *20*). Here, the magnetization is induced through phononic rectification, however, with no magnon mode and spin precession involved. Furthermore, magnons by themselves can induce a magnetization along the equilibrium axis of the spins when the spin-precession amplitudes of the two sublattices differ, as for example in easy-axis antiferromagnets (*37*). The ratio of induced net magnetization to precession amplitude is, however, orders of magnitude smaller compared to the mechanism we describe. Last, there have been reports of nonlinear magnon dynamics by direct excitation with the magnetic field component of light; however, this mechanism also does not involve rectification of spin precession (*71*–*74*).

The mechanism of chiral-phonon–mediated magnonic rectification proposed here enables the generation of a quasi-static spin canting from spin precession and represents a third fundamental rectification process besides optical and phononic rectification. Our example of light-induced magnetization can be seen in the same light as the light-induced generation and control of magnetic order mediated by chiral phonons demonstrated in recent experiments (*31*, *33*, *34*).

Supplementary Materials

This PDF file includes:

Supplementary Text

REFERENCES AND NOTES

1. S. S. Dhillon, M. S. Vitiello, E. H. Linfield, A. G. Davies, M. C. Hoffmann, J. Booske, C. Paoloni, M. Gensch, P. Weightman, G. P. Williams, E. Castro-Camus, D. R. S. Cumming, F. Simoens, I. Escorcia-Carranza, J. Grant, S. Lucyszyn, M. Kuwata-Gonokami, K. Konishi, M. Koch, C. A. Schmuttenmaer, T. L. Cocker, R. Huber, A. G. Markelz, Z. D. Taylor, V. P. Wallace, J. A. Zeitler, J. Sibik, T. M. Korter, B. Ellison, S. Rea, P. Goldsmith, K. B. Cooper, R. Appleby, D. Pardo, P. G. Huggard, V. Krozer, H. Shams, M. Fice, C. Renaud, A. Seeds, A. Stöhr, M. Naftaly, N. Ridler, R. Clarke, J. E. Cunningham, M. B. Johnston, The 2017 terahertz science and technology roadmap. *J. Phys. D Appl. Phys.* **50**, 043001 (2017).
2. M. Först, C. Manzoni, S. Kaiser, Y. Tomioka, Y. Tokura, R. Merlin, A. Cavalleri, Nonlinear phononics as an ultrafast route to lattice control. *Nat. Phys.* **7**, 854–856 (2011).
3. A. Subedi, A. Cavalleri, A. Georges, Theory of nonlinear phononics for coherent light control of solids. *Phys. Rev. B* **89**, 220301(R) (2014).
4. R. Mankowsky, A. Subedi, M. Först, S. O. Mariager, M. Chollet, H. T. Lemke, J. S. Robinson, J. M. Glownia, M. P. Minitti, A. Frano, M. Fechner, N. A. Spaldin, T. Loew, B. Keimer, A. Georges, A. Cavalleri, Nonlinear lattice dynamics as a basis for enhanced superconductivity in $YBa_2Cu_3O_{6.5}$. *Nature* **516**, 71–73 (2014).
5. R. Mankowsky, M. Först, T. Loew, J. Porras, B. Keimer, A. Cavalleri, Coherent modulation of the $YBa_2Cu_3O_{6+x}$ atomic structure by displacive stimulated ionic Raman scattering. *Phys. Rev.* **91**, 094308 (2015).
6. M. Fechner, N. A. Spaldin, Effects of intense optical phonon pumping on the structure and electronic properties of yttrium barium copper oxide. *Phys. Rev. B.* **94**, 134307 (2016).
7. B. Liu, M. Först, M. Fechner, D. Nicoletti, J. Porras, T. Loew, B. Keimer, A. Cavalleri, Pump frequency resonances for light-induced incipient superconductivity in $YBa_2Cu_3O_{6.5}$. *Phys. Rev.* X **10**, 011053 (2020).
8. A. Subedi, Proposal for ultrafast switching of ferroelectrics using midinfrared pulses. *Phys. Rev. B.* **92**, 214303 (2015).
9. R. Mankowsky, A. Von Hoegen, M. Först, A. Cavalleri, Ultrafast reversal of the ferroelectric polarization. *Phys. Rev. Lett.* **118**, 197601 (2017).
10. X. Li, T. Qiu, J. Zhang, E. Baldini, J. Lu, A. M. Rappe, K. A. Nelson, Terahertz field–induced ferroelectricity in quantum paraelectric $SrTiO_3$. *Science* **364**, 1079–1082 (2019).
11. T. F. Nova, A. S. Disa, M. Fechner, A. Cavalleri, Metastable ferroelectricity in optically strained $SrTiO_3$. *Science* **364**, 1075–1079 (2019).
12. V. A. Abalmasov, Ultrafast reversal of the ferroelectric polarization by a midinfrared pulse. *Phys. Rev. B.* **101**, 014102 (2020).
13. P. Chen, C. Paillard, H. J. Zhao, J. Íñiguez, L. Bellaiche, Deterministic control of ferroelectric polarization by ultrafast laser pulses. *Nat. Commun.* **13**, 2566 (2022).
14. M. Henstridge, M. Först, E. Rowe, M. Fechner, A. Cavalleri, Nonlocal nonlinear phononics. *Nat. Phys.* **18**, 457–461 (2022).
15. M. Fechner, A. Sukhov, L. Chotorlishvili, C. Kenel, J. Berakdar, N. A. Spaldin, Magnetophononics: Ultrafast spin control through the lattice. *Phys. Rev. Mater.* **2**, 064401 (2018).
16. G. Khalsa, N. A. Benedek, Ultrafast optically induced ferromagnetic/anti-ferromagnetic phase transition in $GdTiO_3$ from first principles. *NPJ Quantum Mater.* **3**, 15 (2018).
17. M. Gu, J. M. Rondinelli, Nonlinear phononic control and emergent magnetism in Mott insulating titanates. *Phys. Rev. B.* **98**, 024102 (2018).
18. P. G. Radaelli, Breaking symmetry with light: Ultrafast ferroelectricity and magnetism from three-phonon coupling. *Phys. Rev. B.* **97**, 085145 (2018).
19. M. Rodriguez-Vega, Z.-X. Lin, A. Leonardo, A. Ernst, G. Chaudhary, M. G. Vergniory, G. A. Fiete, Phonon-mediated dimensional crossover in bilayer CrI_3. *Phys. Rev. B.* **102**, 081117(R) (2020).
20. A. S. Disa, M. Fechner, T. F. Nova, B. Liu, M. Först, D. Prabhakaran, P. G. Radaelli, A. Cavalleri, Polarizing an antiferromagnet by optical engineering of the crystal field. *Nat. Phys.* **16**, 937–941 (2020).
21. D. Afanasiev, J. R. Hortensius, B. A. Ivanov, A. Sasani, E. Bousquet, Y. M. Blanter, R. V. Mikhaylovskiy, A. V. Kimel, A. D. Caviglia, Ultrafast control of magnetic interactions via light-driven phonons. *Nat. Mater.* **20**, 607–611 (2021).
22. M. Rodriguez-Vega, Z.-X. Lin, A. Leonardo, A. Ernst, M. G. Vergniory, G. A. Fiete, Light-Driven topological and magnetic phase transitions in thin layer antiferromagnets. *J. Phys. Chem. Lett.* **13**, 4152–4158 (2022).
23. A. S. Disa, J. Curtis, M. Fechner, A. Liu, A. Von Hoegen, M. Först, T. F. Nova, P. Narang, A. Maljuk, A. V. Boris, B. Keimer, A. Cavalleri, Photo-induced high-temperature ferromagnetism in $YTiO_3$. *Nature* **617**, 73–78 (2023).
24. T. F. Nova, A. Cartella, A. Cantaluppi, M. Först, D. Bossini, R. V. Mikhaylovskiy, A. V. Kimel, R. Merlin, A. Cavalleri, An effective magnetic field from optically driven phonons. *Nat. Phys.* **13**, 132–136 (2017).
25. D. M. Juraschek, M. Fechner, A. V. Balatsky, N. A. Spaldin, Dynamical multiferroicity. *Phys. Rev. Mater.* **1**, 014401 (2017).
26. D. M. Juraschek, N. A. Spaldin, Orbital magnetic moments of phonons. *Phys. Rev. Mater.* **3**, 064405 (2019).
27. D. M. Juraschek, P. Narang, N. A. Spaldin, Phono-magnetic analogs to opto-magnetic effects. *Phys. Rev. Res.* **2**, 043035 (2020).
28. R. M. Geilhufe, V. Juričić, S. Bonetti, J.-X. Zhu, A. V. Balatsky, Dynamically induced magnetism in $KTaO_3$. *Phys. Rev. Res.* **3**, L022011 (2021).
29. D. M. Juraschek, T. Neuman, P. Narang, Giant effective magnetic fields from optically driven chiral phonons in 4*f* paramagnets. *Phys. Rev. Res.* **4**, 013129 (2022).
30. G. Xiong, H. Chen, D. Ma, L. Zhang, Effective magnetic fields induced by chiral phonons. *Phys. Rev. B.* **106**, 144302 (2022).
31. M. Basini, M. Pancaldi, B. Wehinger, M. Udina, V. Unikandanunni, T. Tadano, M. C. Hoffmann, A. V. Balatsky, S. Bonetti, Terahertz electric-field-driven dynamical multiferroicity in $SrTiO_3$. *Nature* **628**, 534–539 (2024).
32. R. M. Geilhufe, W. Hergert, Electron magnetic moment of transient chiral phonons in $KTaO_3$. *Phys. Rev. B.* **107**, L020406 (2023).
33. C. S. Davies, F. G. N. Fennema, A. Tsukamoto, I. Razdolski, A. V. Kimel, A. Kirilyuk, Phononic switching of magnetization by the ultrafast Barnett effect. *Nature* **628**, 540–544 (2024).
34. J. Luo, T. Lin, J. Zhang, X. Chen, E. R. Blackert, R. Xu, B. I. Yakobson, H. Zhu, Large effective magnetic fields from chiral phonons in rare-earth halides. *Science* **382**, 698–702 (2023).
35. M. F. Nielson, A. Alejandro, S. (Enoch) Ho, M. Lutz, C. D. Moss, J. A. Johnson, "Inducing magnetism in $LiNbO_3$" in *CLEO 2023*, Technical Digest Series (Optica Publishing Group, 2023), paper JTh2A.103.
36. S.-W. Cheong, M. Mostovoy, Multiferroics: A magnetic twist for ferroelectricity. *Nat. Mater.* **6**, 13–20 (2007).
37. S. M. Rezende, A. Azevedo, R. L. Rodríguez-Suárez, Introduction to antiferromagnetic magnons. *J. Appl. Phys.* **126**, 151101 (2019).
38. L. Zhang, Q. Niu, Chiral phonons at high-symmetry points in monolayer hexagonal lattices. *Phys. Rev. Lett.* **115**, 115502 (2015).
39. H. Zhu, J. Yi, M. Y. Li, J. Xiao, L. Zhang, C. W. Yang, R. A. Kaindl, L. J. Li, Y. Wang, X. Zhang, Observation of chiral phonons. *Science* **359**, 579–582 (2018).
40. K. Ishito, H. Mao, Y. Kousaka, Y. Togawa, S. Iwasaki, T. Zhang, S. Murakami, J.-I. Kishine, T. Satoh, Truly chiral phonons in α-HgS. *Nat. Phys.* **19**, 35–39 (2023).
41. H. Ueda, M. García-Fernández, S. Agrestini, C. P. Romao, J. Van Den Brink, N. A. Spaldin, K.-J. Zhou, U. Staub, Chiral phonons in quartz probed by x-rays. *Nature* **618**, 946–950 (2023).
42. D. Shin, H. Hübener, U. De Giovannini, H. Jin, A. Rubio, N. Park, Phonon-driven spin-Floquet magneto-valleytronics in MoS_2. *Nat. Commun.* **9**, 638 (2018).
43. B. Cheng, T. Schumann, Y. Wang, X. Zhang, D. Barbalas, S. Stemmer, N. P. Armitage, A large effective phonon magnetic moment in a Dirac semimetal. *Nano Lett.* **20**, 5991–5996 (2020).
44. Y. Ren, C. Xiao, D. Saparov, Q. Niu, Phonon magnetic moment from electronic topological magnetization. *Phys. Rev. Lett.* **127**, 186403 (2021).
45. A. Baydin, F. G. G. Hernandez, M. Rodriguez-Vega, A. K. Okazaki, F. Tay, G. T. Noe, I. Katayama, J. Takeda, H. Nojiri, P. H. O. Rappl, E. Abramof, G. A. Fiete, J. Kono, Magnetic control of soft chiral phonons in PbTe. *Phys. Rev. Lett.* **128**, 075901 (2022).
46. F. G. G. Hernandez, A. Baydin, S. Chaudhary, F. Tay, I. Katayama, J. Takeda, H. Nojiri, A. K. Okazaki, P. H. O. Rappl, E. Abramof, M. Rodriguez-Vega, G. A. Fiete, J. Kono, Observation of interplay between phonon chirality and electronic band topology. *Sci. Adv.* **9**, eadj4074 (2023).
47. S. Zhang, Y. Pei, S. Hu, N. Wu, D.-Q. Chen, C. Lian, S. Meng, Light-induced phonon-mediated magnetization in monolayer MoS_2. *Chin. Phys. Lett.* **40**, 077502 (2023).
48. J. Fransson, Chiral phonon induced spin polarization. *Phys. Rev. Res.* **5**, L022039 (2023).
49. A. Rückriegel, S. Streib, G. E. W. Bauer, R. A. Duine, Angular momentum conservation and phonon spin in magnetic insulators. *Phys. Rev. B.* **101**, 104402 (2020).
50. M. Hamada, S. Murakami, Conversion between electron spin and microscopic atomic rotation. *Phys. Rev. Res.* **2**, 023275 (2020).
51. S. Chaudhary, D. M. Juraschek, M. Rodriguez-Vega, G. A. Fiete, Giant effective magnetic moments of chiral phonons from orbit-lattice coupling, *Phys. Rev. B.* **110**, 094401 (2024).
52. F. Wu, S. Bao, J. Zhou, Y. Wang, J. Sun, J. Wen, Y. Wan, Q. Zhang, Fluctuation-enhanced phonon magnetic moments in a polar antiferromagnet. *Nat. Phys.* **19**, 1868–1875 (2023).
53. A. Zabalo, C. E. Dreyer, M. Stengel, Rotational *g* factors and Lorentz forces of molecules and solids from density functional perturbation theory. *Phys. Rev. B.* **105**, 094305 (2022).
54. T. Kampfrath, A. Sell, G. Klatt, A. Pashkin, S. Mährlein, T. Dekorsy, M. Wolf, M. Fiebig, A. Leitenstorfer, R. Huber, Coherent terahertz control of antiferromagnetic spin waves. *Nat. Photonics* **5**, 31–34 (2011).
55. T. L. Gilbert, Classics in magnetics A phenomenological theory of damping in ferromagnetic materials. *IEEE Trans. Magn.* **40**, 3443–3449 (2004).
56. B. Skubic, J. Hellsvik, L. Nordström, O. Eriksson, A method for atomistic spin dynamics simulations: Implementation and examples. *J. Phys. Condens. Matter* **20**, 315203 (2008).

57. D. M. Juraschek, S. F. Maehrlein, Sum-frequency ionic Raman scattering. *Phys. Rev. B* **97**, 174302 (2018).
58. D. M. Juraschek, D. S. Wang, P. Narang, Sum-frequency excitation of coherent magnons. *Phys. Rev. B* **103**, 094407 (2021).
59. M. Bass, P. A. Franken, J. F. Ward, G. Weinreich, Optical rectification. *Phys. Rev. Lett.* **9**, 446–448 (1962).
60. R. F. Boyd, *Nonlinear Optics* (Academic Press, Inc., Amsterdam, Boston, 2008).
61. D. Nicoletti, A. Cavalleri, Nonlinear light–matter interaction at terahertz frequencies. *Adv. Opt. Photonics* **8**, 401–464 (2016).
62. A. S. Disa, T. F. Nova, A. Cavalleri, Engineering crystal structures with light. *Nat. Phys.* **17**, 1087–1092 (2021).
63. C. Vicario, A. Trisorio, S. Allenspach, C. Rüegg, F. Giorgianni, Narrow-band and tunable intense terahertz pulses for mode-selective coherent phonon excitation. *Appl. Phys. Lett.* **117**, 101101 (2020).
64. C. Tzschaschel, K. Otani, R. Iida, T. Shimura, H. Ueda, S. Günther, M. Fiebig, T. Satoh, Ultrafast optical excitation of coherent magnons in antiferromagnetic NiO. *Phys. Rev. B* **95**, 174407 (2017).
65. M. Eibschütz, S. Shtrikman, D. Treves, Mössbauer studies of Fe^{57} in orthoferrites. *Phys. Rev.* **156**, 562–577 (1967).
66. D. Lujan, J. Choe, S. Chaudhary, G. Ye, C. Nnokwe, M. Rodriguez-Vega, J. He, F. Y. Gao, T. N. Nunley, E. Baldini, J. Zhou, G. A. Fiete, R. He, X. Li, Spin–orbit exciton–induced phonon chirality in a quantum magnet. *Proc. Natl. Acad. Sci. U.S.A.* **121**, e2304360121 (2024).
67. S. Baierl, J. H. Mentink, M. Hohenleutner, L. Braun, T.-m. Do, C. Lange, A. Sell, M. Fiebig, G. Woltersdorf, T. Kampfrath, R. Huber, Terahertz-driven nonlinear spin response of antiferromagnetic nickel oxide. *Phys. Rev. Lett.* **117**, 197201 (2016).
68. A. M. Kalashnikova, A. V. Kimel, R. V. Pisarev, V. N. Gridnev, A. Kirilyuk, T. Rasing, Impulsive generation of coherent magnons by linearly polarized light in the easy-plane antiferromagnet $FeBO_3$. *Phys. Rev. Lett.* **99**, 167205 (2007).
69. T. G. H. Blank, K. A. Grishunin, B. A. Ivanov, E. A. Mashkovich, D. Afanasiev, A. V. Kimel, Empowering control of antiferromagnets by THz-Induced spin coherence. *Phys. Rev. Lett.* **131**, 096701 (2023).
70. T. G. H. Blank, E. A. Mashkovich, K. A. Grishunin, C. F. Schippers, M. V. Logunov, B. Koopmans, A. K. Zvezdin, A. V. Kimel, Effective rectification of terahertz electromagnetic fields in a ferrimagnetic iron garnet. *Phys. Rev. B* **108**, 094439 (2023).
71. E. A. Mashkovich, K. A. Grishunin, R. M. Dubrovin, A. K. Zvezdin, R. V. Pisarev, A. V. Kimel, Terahertz light–driven coupling of antiferromagnetic spins to lattice. *Science* **374**, 1608–1611 (2021).
72. T. Kurihara, M. Bamba, H. Watanabe, M. Nakajima, T. Suemoto, Observation of terahertz-induced dynamical spin canting in orthoferrite magnon by magnetorefractive probing. *Commun. Phys.* **6**, 51 (2023).
73. Z. Zhang, F. Y. Gao, Y.-C. Chien, Z.-J. Liu, J. B. Curtis, E. R. Sung, X. Ma, W. Ren, S. Cao, P. Narang, A. Von Hoegen, E. Baldini, K. A. Nelson, Terahertz-field-driven magnon upconversion in an antiferromagnet. *Nat. Phys.* **20**, 788–793 (2024).
74. Z. Zhang, F. Y. Gao, J. B. Curtis, Z.-J. Liu, Y.-C. Chien, A. Von Hoegen, M. T. Wong, T. Kurihara, T. Suemoto, P. Narang, E. Baldini, K. A. Nelson, Terahertz field-induced nonlinear coupling of two magnon modes in an antiferromagnet. *Nat. Phys.* **20**, 801–806 (2024).

Acknowledgments: We thank W. Hu for discussions. **Funding:** T.K. and D.M.J. acknowledge support from Tel Aviv University. D.A.B.L. acknowledges support from the US Department of Energy, Office of Science, Office of Basic Energy Sciences Early Career Research Program under award number DE-SC-0021305. Calculations were performed on local computing infrastructure at Tel Aviv University. **Author contributions:** T.K. and D.A.B.L. performed the numerical simulations and analytical derivations. T.K., D.A.B.L., and D.M.J. analyzed and validated the data. T.K. and D.M.J. visualized the data. D.M.J. conceptualized and supervised the project. All authors contributed to writing the manuscript. **Competing interests:** The authors declare that they have no competing interests. **Data and materials availability:** All data required to reach the conclusions of this study are presented in the main text and/or Supplementary Materials. Data and code can be found at https://doi.org/10.5281/zenodo.10888643.

Submitted 15 January 2024
Accepted 16 August 2024
Published 25 September 2024
10.1126/sciadv.ado0722